Transparent superconductivity in lithiated indium tin oxide thin films

Denisse Córdova Carrizales,[1] Rain K. C. Wang,[1] Johanna Nordlander,[1] Grace A. Pan,[1] Erika V. Ortega Ortiz,[1] Larissa Little,[2] Arthur McClelland,[3] Ed Macomber,[3] Austin J. Akey,[3] Jarad A. Mason,[4] Charles M. Brooks,[1] Julia A. Mundy,[1,2] and Ari B. Turkiewicz[1]

[1]*Department of Physics, Harvard University, Cambridge, Massachusetts 02138, USA*
[2]*School of Engineering and Applied Sciences, Harvard University, Cambridge, Massachusetts 02138, USA*
[3]*Center for Nanoscale Systems, Harvard University, Cambridge, Massachusetts 02138, USA*
[4]*Department of Chemistry and Chemical Biology, Harvard University, Cambridge, Massachusetts 02138, USA*

(Received 15 June 2023; accepted 15 November 2024; published 27 December 2024)

Indium tin oxide (Sn-doped In_2O_3; ITO) is a well-studied transparent conductor where doping can be used to stabilize a superconducting state. In this work, we use a combination of thin film deposition of ITO and solution-phase chemistry using *n*-BuLi (C_4H_9Li) to realize superconductivity in Li-doped ITO. Solution-phase intercalation is commonly employed for bulk, polycrystalline materials but has rarely been applied to thin films. Using x-ray diffraction, atomic force microscopy, electronic transport, and optical transmission measurements, we characterize the optical transparency and superconductivity of lithium intercalated ITO thin films. After 72 hours of lithium intercalation, we find a critical temperature, T_c, of 0.49 K and an optical transparency of at least 73% in the visible optical range—all while maintaining crystallinity and nanometer surface roughness.

DOI: 10.1103/PhysRevMaterials.8.124803

I. INTRODUCTION

Transparent superconductivity is a rare and seemingly contradictory physical phenomenon: this phase requires a high enough carrier density, n_e, to stabilize superconductivity yet a low enough density to remain (mostly) optically transparent. Transparent superconductors can be used as high-energy resolution detectors whose superconducting Cooper pairs are broken by small energy depositions to detect α particles, γ-rays, or dark matter [1,2,3]. Furthermore, transparent superconductors have a number of proposed applications in next-generation optoelectronic and computing devices. Transparent superconductors can be used in quantum circuits to reduce decoherence [4], reduce quasiparticle formation [5], and improve electro-optical transduction [6,7]—all necessary for future quantum information networks [6]. The key to realizing these proposed optoelectronic and computing applications is the identification of new, scalable, optically transparent superconducting materials and methods to synthesize them.

Indium tin oxide (Sn-doped In_2O_3; ITO) is one of the most commonly used transparent conductors [8]; it is a degenerately doped semiconductor with an optical transparency of more than 80% in the visible range and a resistivity on the order of $10^{-4}\,\Omega$ cm at 20 °C [8,9,10]. Superconductivity below 5 K in ITO can be realized by introducing oxygen vacancies or ions, raising the carrier concentration to at least 10^{21} cm^{-3} [11,12]. The band gap in ITO also increases with doping, keeping interband transitions from the valence band out of the optical range [9].

Large interatomic spacings make ITO an attractive target to insert small ions into. Crystalline ITO (100) thin films have been electrochemically intercalated with sodium to realize a superconducting state by Aliev *et al.* [12]. The critical temperature, T_c, in Na-doped ITO exhibits dome-shaped behavior as a function of carrier density—peaking at ∼5 K [12]. Na-doped ITO remains partially transparent to visible light at 20 °C [12], making it a transparent superconductor. The T_cs of crystalline indium, crystalline tin, and amorphous indium oxide (In_2O_3) are 3.4 K [13,14], 3.7 K [13,15], and 0.3 K [16], respectively, while crystalline indium oxide does not superconduct [17]. Electrochemical lithium intercalation of ITO thin films has also been reported, but only the optical properties are described [18]. Both the electrical transport and optical transmittance properties of Li-doped ITO have yet to be reported.

Here, we realize superconductivity in sputtered indium tin oxide epitaxial thin films after using solution-phase chemistry to intercalate them with lithium. Solution-phase intercalation is commonly employed for bulk, polycrystalline materials but has rarely been applied to thin films. For the intercalation step, we employ solution-phase *n*-BuLi (C_4H_9Li) to chemically reduce the ITO thin films in place of using electrochemistry. This solution-phase intercalation validates a method for intercalating ions into ITO thin films at low temperature and without an electric potential. Following lithium intercalation into the ITO, we find a T_c of 0.49 K with a critical field, H_c, of 0.03 T. We also observe optical transparency of at least 73% in the 400 nm to 750 nm wavelength range at 20 °C. In this work, we illustrate that solution-phase chemistry can be used to intercalate relevant species across the area of a thin film and elicit new electronic phenomena by measuring superconductivity over macroscopic distances.

II. EXPERIMENTAL METHODS

A. Synthesis of ITO films with reactive sputtering

We used an Orion 3 AJA International sputtering system to synthesize indium tin oxide (ITO) thin films onto

(111)-oriented yttrium-stabilized zirconia (YSZ) substrates from Crystec. To prepare the substrate surfaces for thin film deposition, we annealed the YSZ for three hours in air at 1300 °C. To ensure thermal uniformity across each substrate during thin film growth, we adhered the substrates with nickel paste onto a sputtering sample holder. Once the sputtering chamber reached a pressure of 1×10^{-6} Torr, we used a radio frequency gun at a deposition power of 80 W to ionize argon gas flowing at 15 sccm. The argon plasma, at a pressure of 1×10^{-3} Torr, then bombarded an ITO target composed of 90% In_2O_3 and 10% SnO_2 by weight.

We deposited a layer of ITO at a substrate temperature of 20 °C for 2 minutes and 45 seconds and then a layer at 500 °C for 12 minutes for a total film thickness of ∼51 nm. The base layer deposited at 20 °C ensured that the thin film grew uniformly across the surface of the substrate [19]. The second layer was deposited at 500 °C since the crystalline quality and transparency of ITO are higher quality at higher growth temperatures [10]. Following the deposition, we cooled the film down to 20 °C at 1×10^{-4} Torr with no gas flow.

B. Solution-phase lithium intercalation

We used *n*-BuLi in a solution of hexanes to intercalate lithium into ITO thin films and conducted all manipulations in a N_2-filled glovebox. We placed samples in individual 20 mL scintillation vials and immersed the samples in 2 mL of a 1.6 M solution of *n*-BuLi in hexanes. The vials were sealed with Teflon-lined caps and heated to 60 °C for 72 hours. The reaction was cooled to 30 °C, and then the solution was decanted and replenished with fresh *n*-BuLi in hexanes every 24 hours. At the end of the total reaction time, the solution was cooled to 30 °C and then decanted. The sample was then immersed in tetrahydrofuran and removed from the glovebox. The tetrahydrofuran was decanted, and the sample was washed with isopropanol to quench residual *n*-BuLi. Finally, the isopropanol was decanted, and the sample was dried using N_2 and stored in a desiccator.

C. Structural characterization

To measure the x-ray diffraction (XRD) pattern of the films, we used a Malvern Panalytical Empyrean diffractometer with a hybrid monochromator and Cu Kα ($\lambda = 1.5406$ Å) radiation. We used a Nelson-Riley fit to extract the lattice parameters of each thin film [20]. We acquired x-ray reflectivity scans to determine film thickness and ϕ scans to determine in-plane orientations on the same instrument. We also acquired reciprocal space maps to determine the strain of the films using a PIXcel3D 2D pixel area detector on the same instrument.

To determine thin film surface roughness and homogeneity, we acquired atomic force microscopy (AFM) images in tapping mode on the MFP-3D Origin+ Asylum Research AFM from Oxford Instruments.

D. Electronic transport

Following lithium intercalation, we used an electron-beam evaporator to deposit contacts (100 nm of gold on top of 5 nm of chromium) patterned with Hall bar geometry shadow masks. We further defined the Hall bar channels with a diamond scribe to ensure electrical isolation between contacts. Given the large size and close spacing of the electrical contacts relative to the area of the underlying film, we acknowledge uncertainties in our calculations of conductivity and carrier concentration. However, these uncertainties do not impact our observation of superconductivity or other qualitative conclusions drawn from electrical resistivity data. Photographs of the Hall bars we used for the electrical measurements are shown in Supplemental Material [21].

We collected electrical resistivity data from 300 K down to 1.8 K in a Quantum Design Physical Property Measurement System with a 9 T magnet using AC (∼15 Hz) lock-in techniques. The low-temperature measurements used a dilution refrigerator insert to reach ∼50 mK. To calculate the carrier densities, we first collected resistance measurements in Hall geometry configurations under magnetic field sweeps up to 9 T at several temperatures. Then we fit our antisymmetrized data (Supplemental Material [21]) to a linear Drude model to extract the carrier density. During these measurements, the film was oriented perpendicular to the magnetic field.

E. Optical transmission

To determine optical transparency, we used an Agilent Technologies Cary 60 UV-Vis system equipped with a silicon photodiode detector and a xenon flashlamp with a 1 mm diameter lamp source. Prior to measurement, we removed the nickel paste used to adhere the substrate to the sputtering sample holder and polished the backside of the sample to optical smoothness using diamond lapping film. We collected light transmitted through the lithiated ITO thin films at 20 °C between the 200 nm to 1100 nm range using a 0.1 second averaging time and 1 nm data spacing in the WinUV software program. We also collected the spectrum from a bare substrate.

III. RESULTS AND DISCUSSION

A. Structural characterization

Using reactive sputtering, we deposited single-phase and epitaxial thin films of ITO on (111) YSZ substrates. Figures 1(a)–1(c) display θ-2θ XRD patterns both for an as-synthesized ITO film and a thin film intercalated for 72 hours. Both before and after intercalation the film is single-phase with an out-of-plane (111) orientation. Following intercalation, the θ-2θ XRD peaks shift to lower angles, consistent with a lattice constant expansion by 1% after lithium intercalation for 72 hours. Aliev *et al*. also report that the volume of the unit cell shows only small changes with the intercalation of sodium [12]. Figures 1(d)–1(e) show the AFM scans of the film before and after intercalation, respectively, demonstrating that the films become rougher after the intercalation although maintain a nanoscale surface roughness.

The ϕ scan (Supplemental Material [21]) demonstrates the in-plane film crystallographic relationship ITO $[11\bar{2}] \parallel [11\bar{2}]$ YSZ substrate although the film is not commensurate with the substrate (Supplemental Material [21]). The Kiessig fringes in the x-ray reflectivity (Supplemental Material [21]) indicate the films are smooth with a coherent interface.

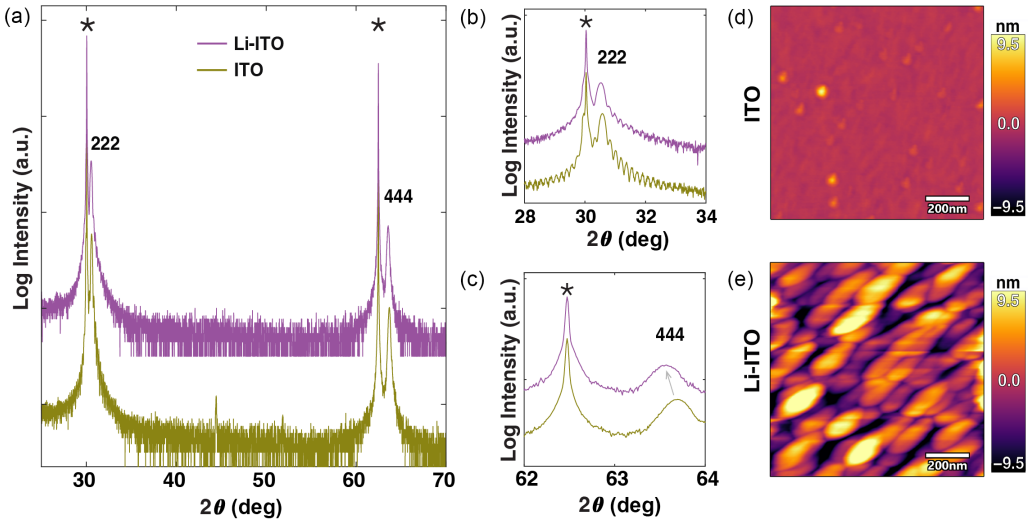

FIG. 1. Comparison of structural properties of pristine ITO thin film and Li-doped ITO thin film intercalated for 72 hours. (a) X-ray diffraction pattern of the as-grown ITO film and the Li-intercalated film. The parent and intercalated films form in the (111) orientation on (111)-oriented YSZ substrate and are phase pure. The peaks present at 45 and 52 degrees in the ITO pattern are from residual nickel paste used during the sputtering process on the underside of the thin film. (b), (c) X-ray diffraction pattern from the film peaks. There is a slight increase in parallel plane spacing in ITO thin film after lithium intercalation, consistent with a slight increase in the lattice parameter. (d) Atomic force microscopy scan before intercalation. The surface roughness is 488.76 pm in the as-grown ITO film. (e) Atomic force microscopy scan after intercalation. The surface roughness is 5.437 nm. After intercalation, repeating oblong islands appear.

We also verify that lithium is indeed present in the film following the intercalation through atom probe tomography (Supplemental Material [21]). While lithium is known to migrate under an applied electric field during tomography experiments [22], these results unambiguously demonstrate lithium incorporation within the film.

B. Electronic transport

Before intercalation, our ITO thin films exhibit metallic behavior down to 2.4 K (Supplemental Material [21]) with resistivities on the order of 10^{-4} Ω cm at 20 °C, consistent with prior reports [11]. The electronic properties of ITO intercalated with lithium for 72 hours are shown in Fig. 2. The Li-intercalated ITO shows an increase in resistivity relative to the resistivity of the parent ITO at 300 K—a relationship also observed in ITO doped with sodium [12]. In our intercalated films, we observe a resistive downturn with an onset at ∼4.5 K (Supplemental Material [21]) and a T_c of 0.49 K. We define the T_c as the temperature at which the resistivity falls to 50% of the normal state resistivity under zero applied magnetic field. The sample reaches a fully superconducting state with zero Ohms at 0.1 K under 0 T [Fig. 2(a)]. We observe a critical magnetic field of $H_C = 0.03$ T at 50 mK. We define the critical

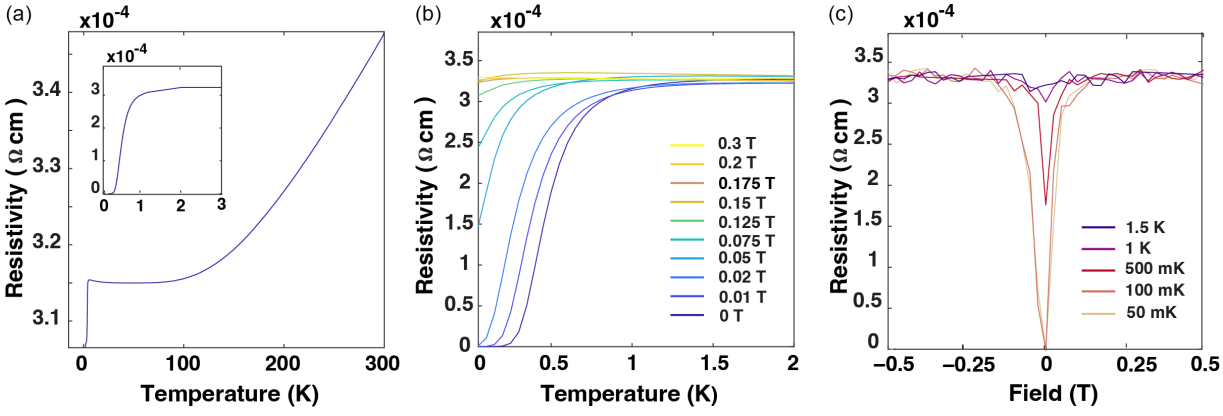

FIG. 2. Superconductivity in an ITO thin film intercalated with lithium for 72 hours. (a) Resistivity as a function of temperature without a magnetic field. The T_c is 0.49 K. We define the T_c as the temperature at which the resistivity falls to 50% of the normal state resistivity under zero applied magnetic field. The Li-doped ITO sample reaches zero resistivity at 0.1 K (inset). The film has a residual-resistivity ratio of 1.94 with resistivities measured at 300 K and 0.51 K. (b) Resistivity as a function of temperature in an applied magnetic field for the film shown in (a). A magnetic field of 0.3 T fully suppresses the superconducting behavior of the sample. (c) R-H curves for the sample as a function of temperature for the film shown in (a). The critical magnetic field H_c is 0.03 T. We define the critical magnetic field as the applied magnetic field under which the Li-doped ITO reaches 50% of its normal state resistivity while cooled to 50 mK.

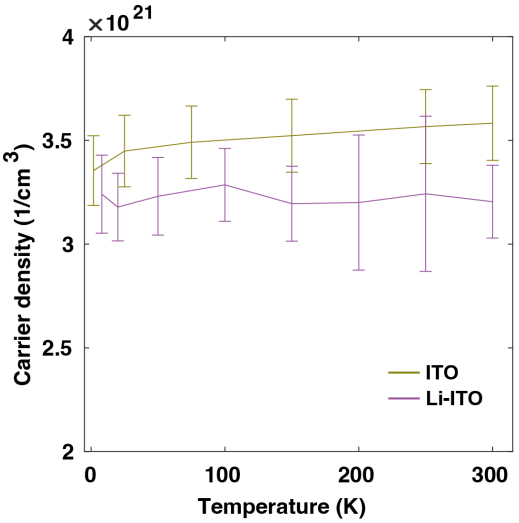

FIG. 3. Carrier density over 1.8 K to 300 K temperature range for an as-grown ITO thin film and a Li-doped ITO thin film intercalated for 72 hours. We assume a 5% error in the measurement of film thickness from x-ray reflectivity to determine the carrier density error bars.

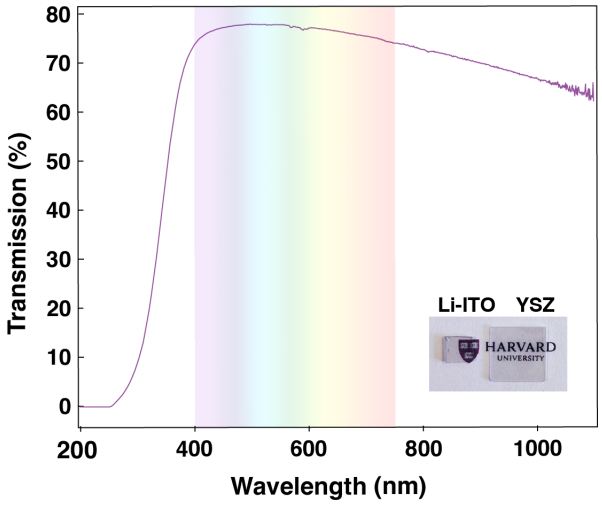

FIG. 4. Optical transmission spectrum for ITO film intercalated for 72 hours on YSZ substrate at 20 °C. The sample shows $\geqslant$ 73% transmission throughout the visible range. The inset shows a photograph of the Li-doped ITO film and bare YSZ substrate.

magnetic field as the applied magnetic field under which the Li-doped ITO reaches 50% of its normal state resistivity while cooled to 50 mK. We also calculated the in-plane coherence length to be $\xi_{ab} = 75 \pm 2$ nm (Supplemental Material [21]).

After lithium intercalation for 72 hours, the carrier density of our ITO thin films is on the order of 10^{21} cm^{-3} (Fig. 3). We observe that the carrier density of the ITO film decreases after intercalation with lithium—a relationship similarly observed in indium oxide after being doped with zinc oxide to achieve superconductivity [23].

C. Optical transmission

The undoped ITO compound is a well-studied transparent conductor, and following intercalation, our films retain high optical transparency. Visually, we observe a light blue tint on the film, which agrees with Zhang *et al.* [18]. The optical properties of ITO intercalated with lithium for 72 hours are shown in Fig. 4. The optical transparency peaks at 78% at ∼500 nm and maintains at least 73% transparency through the visible optical range, comparable to that of the YSZ substrate over most of the visible range (Supplemental Material [21]). These visible optical transparency results are within the range reported for the electrochemical injection of lithium into ITO [18].

IV. CONCLUSION

We have synthesized transparent superconducting Li-doped ITO through thin film synthesis and solution-phase chemistry—which has rarely been applied to thin films. To our knowledge, this is the first time that transparent superconducting Li-doped ITO has been characterized. We used solution-phase *n*-BuLi to intercalate lithium ions into this oxide system and achieve a T_c of 0.49 K while retaining an optical transparency of at least 73% in the visible range. While *n*-BuLi has previously been used in bulk materials systems to discover new superconducting phases [24,25,26,27], we have demonstrated its viability to achieve superconductivity in the crystalline thin film ITO system, with potential applications across other thin film materials systems.

ACKNOWLEDGMENTS

The authors wish to acknowledge useful conversations with Jennifer Hoffman and Emma Batson. This work was supported by the National Science Foundation (Grant No. OMA-2137723) and the Center for Quantum Networks (Grant No. EEC-1941583). Film deposition, nanofabrication, optical characterization, and atom probe topography work was performed in part at Harvard University's Center for Nanoscale Systems (CNS), a member of the National Nanotechnology Coordinated Infrastructure Network (NNCI), supported by the National Science Foundation under NSF Grant No. 1541959. D.C.C. acknowledges support from the Harvard Quantum Initiative. J.N. acknowledges support from the Swiss National Science Foundation under Project No. P2EZP2-195686. G.A.P. acknowledges support from the NSF Graduate Research Fellowship Grant No. DGE-1745303. J. A. Mundy acknowledges support from the Packard Foundation and the Sloan Foundation.

[1] E. C. Crittenden and D. E. Spiel, Superconducting thin-film detector of nuclear particles, J. Appl. Phys. **42**, 3182 (1971).

[2] N. E. Booth, B. Cabrera, and E. Fiorini, Low temperature particle detectors, Annu. Rev. Nucl. Part. Sci. **46**, 471 (1996).

[3] F. Simon, Application of low temperature calorimetry to radioactive measurements, Nature (London) **135**, 763 (1935).

[4] R. Barends, J. Wenner, M. Lenander, Y. Chen, R. C. Bialczak, J. Kelly, E. Lucero, P. O'Malley, M. Mariantoni, D. Sank, H. Wang, T. C. White, Y. Yin, J. Zhao, A. N. Cleland, J. M. Martinis, and J. J. A. Baselmans, Loss and decoherence due to stray infrared light in superconducting quantum circuits, Appl. Phys. Lett. **99**, 113507 (2011).

[5] R. P. Budoyo, J. B. Hertzberg, C. J. Ballard, K. D. Voigt, Z. Kim, J. R. Anderson, C. J. Lobb, and F. C. Wellstood, Effects of nonequilibrium quasiparticles in a thin-film superconducting microwave resonator under optical illumination, Phys. Rev. B **93**, 024514 (2016).

[6] A. Rueda, F. Sedlmeir, M. C. Collodo, U. Vogl, B. Stiller, G. Schunk, D. V. Strekalov, C. Marquardt, J. M. Fink, O. Painter, G. Leuchs, and H. G. L. Schwefel, Efficient microwave to optical photon conversion: An electro-optical realization, Optica **3**, 597 (2016).

[7] J. Holzgrafe, N. Sinclair, D. Zhu, A. Shams-Ansari, M. Colangelo, Y. Hu, M. Zhang, K. K. Berggren, and M. Lončar, Cavity electro-optics in thin-film lithium niobate for efficient microwave-to-optical transduction, Optica **7**, 1714 (2020).

[8] P. P. Edwards, A. Porch, M. O. Jones, D. V. Morgan, and R. M. Perks, Basic materials physics of transparent conducting oxides, Dalton Transactions, 2995 (2004).

[9] O. N. Mryasov and A. J. Freeman, Electronic band structure of indium tin oxide and criteria for transparent conducting behavior, Phys. Rev. B **64**, 233111 (2001).

[10] I. Hamberg and C. G. Granqvist, Evaporated Sn-doped In_2O_3 films: Basic optical properties and applications to energy-efficient windows, J. Appl. Phys. **60**, R123 (1986).

[11] N. Mori, Superconductivity in transparent Sn-doped In_2O_3 films, J. Appl. Phys. **73**, 1327 (1993).

[12] A. E. Aliev, K. Xiong, K. Cho, and M. B. Salamon, Reversible superconductivity in electrochromic indium-tin oxide films, Appl. Phys. Lett. **101**, 252603 (2012).

[13] M. F. Merriam and M. Von Herzen, Superconductivity in the indium-tin System, Phys. Rev. **131**, 637 (1963).

[14] J. G. Daunt, A. Horseman, and K. Mendelssohn, LXX. Thermodynamical properties of some supraconductors, London Edinburgh Philos. Mag. & J. Sci. **27**, 754 (1939).

[15] H. London, The high-frequency resistance of superconducting tin, Proc. R. Soc. London A: Math. Physical Sci. **176**, 522 (1940).

[16] D. Kowal and Z. Ovadyahu, Scale dependent superconductor–insulator transition, Physica C: Superconductivity **468**, 322 (2008).

[17] W. Seiler, M. Nistor, C. Hebert, and J. Perrière, Epitaxial undoped indium oxide thin films: Structural and physical properties, Sol. Energy Mater. Sol. Cells **116**, 34 (2013).

[18] B. Zhang, G. Xu, S. Tan, and C. Liu, Effects of indium-doped tin oxide film on electrochromic properties under lithium ion guidance, Opt. Mater. (Amsterdam) **101**, 109756 (2020).

[19] X. W. Sun, H. C. Huang, and H. S. Kwok, On the initial growth of indium tin oxide on glass, Appl. Phys. Lett. **68**, 2663 (1996).

[20] J. B. Nelson and D. P. Riley, An experimental investigation of extrapolation methods in the derivation of accurate unit-cell dimensions of crystals, Proc. Phys. Soc. **57**, 160 (1945).

[21] See Supplemental Material at http://link.aps.org/supplemental/10.1103/PhysRevMaterials.8.124803 for photographs of Hall bar devices of ITO and Li-ITO; antisymmetrized resistivities for ITO; in-plane orientation phi scans of Li-ITO and YSZ substrate; reciprocal space map of Li-ITO and YSZ substrate; x-ray reflectivity measurements of as-grown ITO; atom probe tomography; coherence length calculation; electronic properties of ITO and Li-ITO; and optical transmission spectrum of YSZ substrate, which also includes Refs. [22,28–35].

[22] S.-H. Kim, S. Antonov, X. Zhou, L. T. Stephenson, C. Jung, A. A. El-Zoka, D. K. Schreiber, M. Conroy, and B. Gault, Atom probe analysis of electrode materials for Li-ion batteries: Challenges and ways forward, J. Mater. Chem. A **10**, 4926 (2022).

[23] K. Makise, N. Kokubo, S. Takada, T. Yamaguti, S. Ogura, K. Yamada, B. Shinozaki, K. Yano, K. Inoue, and H. Nakamura, Superconductivity in transparent zinc-doped In_2O_3 films having low carrier density, Sci. Technol. Adv. Mater. **9**, 044208 (2008).

[24] Y. Nozuyama and S. Iida, Superconductivity in lithium intercalated 1T– and 4Hb–TaS_2, Jpn. J. Appl. Phys. **23**, L319 (1984).

[25] Y. Ōnuki, S. Yamanaka, R. Inada, M. Kido, and S. Tanuma, Superconductivity of alkali metal intercalated $ZrSe_2$, Synth. Met. **5**, 245 (1983).

[26] C. S. McEwen, D. J. St. Julien, P. P. Edwards, and M. J. Sienko, Structure and superconductivity in lithium-intercalated niobium dichalcogenides, Inorg. Chem. **24**, 1656 (1985).

[27] M. Alario-Franco, Lithium insertion in $Ba_2YCu_3O_{7-y}$, Solid State Ionics **44**, 73 (1990).

[28] M. J. R. Sandim, D. Tytko, A. Kostka, P. Choi, S. Awaji, K. Watanabe, and D. Raabe, Grain boundary segregation in a bronze-route Nb_3Sn superconducting wire studied by atom probe tomography, Supercond. Sci. Technol. **26**, 055008 (2013).

[29] K. Hoummada, F. Dahlem, F. Panciera, E. Bustarret, C. Marcenat, D. Débarre, Y. El Amraoui, and D. Mangelinck, Analysis of superconducting silicon epilayers by atom probe tomography: Composition and evaporation field, Eur. Phys. J. Appl. Phys. **98**, 40 (2023).

[30] V. Heera, J. Fiedler, M. Naumann, R. Skrotzki, S. Kölling, L. Wilde, T. Herrmannsdörfer, W. Skorupa, J. Wosnitza, and M. Helm, Depth-resolved transport measurements and atom-probe tomography of heterogeneous, superconducting Ge:Ga films, Supercond. Sci. Technol. **27**, 055025 (2014).

[31] S. Pedrazzini, A. J. London, B. Gault, D. Saxey, S. Speller, C. R. M. Grovenor, M. Danaie, M. P. Moody, P. D. Edmondson, and P. A. J. Bagot, Nanoscale stoichiometric analysis of a high-temperature superconductor by atom probe tomography, Microsc. Microanal. **23**, 414 (2017).

[32] N. Banno, T. Takeuchi, and K. Tsuchiya, Microstructural observation of transformed Nb_3 Al superconductors using TEM and atom probe tomography, IEEE Trans. Appl. Supercond. **24**, 1 (2014).

[33] Y.-J. Kim, R. Tao, R. F. Klie, and D. N. Seidman, Direct atomic-scale imaging of hydrogen and oxygen interstitials in pure niobium using atom-probe tomography and aberration-

corrected scanning transmission electron microscopy, ACS Nano **7**, 732 (2013).

[34] K. Hoummada, F. Dahlem, T. Kociniewski, J. Boulmer, C. Dubois, G. Prudon, E. Bustarret, H. Courtois, D. Débarre, and D. Mangelinck, Absence of boron aggregates in superconducting silicon confirmed by atom probe tomography, Appl. Phys. Lett. **101**, 182602 (2012).

[35] N. R. Werthamer, E. Helfand, and P. C. Hohenberg, Temperature and purity dependence of the superconducting critical field, H_{c2}. III. Electron spin and spin-orbit effects, Phys. Rev. **147**, 295 (1966).